LAWRENCE
LIVERMORE
NATIONAL
LABORATORY

UCRL-JRNL-234653

Radionuclide Transport in Fracture-Granite Interface Zones

Q. Hu, A. Mori

September 17, 2007

Physics and Chemistry of the Earth

Radionuclide transport in fracture-granite interface zones

Q. H. Hu[a*], A. Möri [b]

[a] Chemical Sciences Division, Lawrence Livermore National Laboratory, 7000 East Avenue, Livermore, CA 94550, USA

[b] Institute of Geological Sciences, University of Bern, Switzerland

Prepared for

Physics and Chemistry of the Earth

* Corresponding author. Tel.: +1 925 422 6774; fax: +1 925 422 3160. E-mail address: hu7@llnl.gov (Q.H. Hu)

Abstract

In situ radionuclide migration experiments, followed by excavation and sample characterization, were conducted in a water-conducting shear zone at the Grimsel Test Site (GTS) in Switzerland to study diffusion paths of radionuclides in fractured granite. In this work, we employed a micro-scale mapping technique that interfaces laser ablation sampling with inductively coupled plasma-mass spectrometry (LA/ICP-MS) to measure the fine-scale (micron-range) distribution of actinides (^{234}U, ^{235}U, and ^{237}Np) in the fracture-granite interface zones. Long-lived ^{234}U, ^{235}U, and ^{237}Np were detected in flow channels, as well as in the adjacent rock matrix, using the sensitive, feature-based mapping of the LA/ICP-MS technique. The injected sorbing actinides are mainly located within the advective flowing fractures and the immediately adjacent regions. The water-conducting fracture studied in this work is bounded on one side by mylonite and the other by granitic matrix regions. These actinides did not penetrate into the mylonite side as much as the relatively higher-porosity granite matrix, most likely due to the low porosity, hydraulic conductivity, and diffusivity of the fracture wall (a thickness of about 0.4 mm separates the mylonite region from the fracture) and the mylonite region itself. Overall, the maximum penetration depth detected with this technique for the more diffusive ^{237}Np over the field experimental time scale of about 60 days was about 10 mm in the granitic matrix, illustrating the importance of matrix diffusion in retarding radionuclide transport from the advective fractures. Laboratory tests and numerical modeling of radionuclide diffusion into granitic matrix was conducted to complement and help interpret the field results. Measured apparent diffusivity of multiple tracers in granite provided consistent predictions for radionuclide transport in the fractured granitic rock.

Keywords: radionuclide, diffusion, transport, granite, Grimsel Test Site.

1. **Introduction**

Matrix diffusion in fractured rocks is recognized as an important process in retarding radionuclide transport. In the last three decades, there has been an increased appreciation of the importance of matrix diffusion in the subsurface transport of solutes (e.g., Neretnieks, 1980; Grisak and Pickens, 1980; Abelin et al., 1991; Maloszewski and Zuber, 1993; Novakowski and Lapcevic, 1994; Hadermann and Herr, 1996; Meigs and Beauheim, 2001; Hu et al., 2001; Salve et al., 2004; Zhou et al., 2006; Möri et al., 2006; Dai et al., 2007). However, there have been few long-term field-scale experiments to realistically evaluate the matrix diffusion of actual radionuclides in fractured rock with minimal disturbance to the *in situ* condition. Changes to the pore spaces near the fractures (alteration and deformation halos), and the presence of a complex system of cracks and altered minerals deep within the unaltered matrix, will influence the radionuclide distribution and residence time in the rock matrix (Sardini et al., 2006). This research is part of an ongoing long-term diffusion (LTD) project to further study the large-scale *in situ* diffusion of radionuclides in fractured rocks.

The Grimsel Test Site (GTS) is an underground rock laboratory that has been operated since 1984 by the Swiss National Co-operative for the Disposal of Radioactive Waste (NAGRA). It is the only field site in the world where radionuclides are permitted to be released for underground experiments, and thus it has been used over the past two decades for various transport studies of radionuclide migration and interactions with fractured repository host rocks, such as granite (Alexander et al, 1992; Hadermann and Heer, 1996; Eikenberg et al., 1998; Frieg et al., 1998; Smith et al., 2001). Migration experiments on radionuclides, including sorbing ^{137}Cs and other non-sorbing and/or short-lived radionuclides, had been conducted since 1988 in a shear zone located in the granodioritic host rock at the GTS. The shear zone consists of an array of

cleavage parallel fracture planes that are mainly filled with fault breccia and/or fine-grained cohesionless fault gauge, and mica-rich mylonite bands that experienced brittle reactivation (cf., Möri et al., 2006). In 1996, a number of *in situ* tracer tests were performed by injecting radionuclides, including long-lived $^{234/235}$U and ^{237}Np, into a saturated dipole flow field with a length of 1.7 m. Injection and extraction flow rates were constant at 8.1±0.2 and 158±1 mL/min, respectively (Eikenberg et al., 1998). Two months later, the flow field was impregnated with fluoresceine-doped epoxy resin to identify *in situ* flow channels and then excavated by overcoring with two 300 mm boreholes parallel to the shear zone. Some of the drill cores were sliced and radionuclide (^{60}Co and ^{137}Cs) retardation sites along the flow paths were detected by β/γ-autoradiography (Möri et al., 2006).

In this work, we use some of the drill core samples to investigate the effects of structural/mineralogical features in fracture-matrix interface zones on matrix diffusion of radionuclides (long-lived ^{234}U, ^{235}U, and ^{237}Np) in fractured granite. Using a sensitive, multi-elemental, micro-scale mapping technique (Hu et al., 2004) that interfaces laser ablation sampling with inductively coupled plasma-mass spectrometry (LA/ICP-MS), we determined the distribution of these actinides across the shear zone. Laboratory tests and numerical modeling of radionuclide diffusion into granitic matrix was conducted to complement and help interpret the field results by determining diffusion and sorption rates.

2. Materials and methods

2.1 Laboratory diffusion test

Both non-radioactive species, or surrogates, and radionuclides (^{235}U, ^{237}Np, and ^{242}Pu) were employed in investigating the diffusion and sorption processes of radionuclides in the GTS granite. Surrogates were chosen based on their chemical similarity to radionuclides of interest.

Non-radioactive cesium and strontium were substituted for radioactive ^{137}Cs and ^{90}Sr. Perrhenate (ReO_4^-) served as an analog for $^{99}TcO_4^-$ (Brookins, 1986) and nickel for cobalt (Eikenberg et al., 1998). These radionuclides (^{60}Co, ^{90}Sr, ^{99}Tc, ^{137}Cs, ^{237}Np, and uranium and plutonium isotopes) were studied because their presence could pose health risks at sites contaminated by nuclear operations and geological repositories for storing nuclear waste (NRC 2000; Zhang et al., 2002).

Saturated diffusion tests were conducted to investigate tracer diffusion into cylindrical (10 mm wide and 10 mm high) GTS granite samples, which had been fully saturated (with the help of vacuum pulling) with a dilute Na-K-HCO_3-type groundwater. The saturated sample was placed on a Teflon mesh inside a chamber such that only the bottom portion was in contact with the tracer solution (to minimize hydraulic head difference), which was stirred constantly with a magnetic stirrer. To maintain a nearly constant tracer concentration, the solution reservoir is large—up to 800 mL—compared to < 0.01 mL pore volume of the sample. The lidded chamber was placed inside an incubator with a controlled temperature of 23 $^{\circ}$C. After a particular diffusion duration (~20 hrs for this granite), we stopped the diffusion by placing the sample inside a -80 $^{\circ}$C freezer, which was followed by freezer-drying and dry storing for LA/ICP-MS analysis. Instead of the commonly used through-diffusion approach in which the tracer concentrations in the source and/or sink reservoirs are measured, we directly mapped the tracer concentration distribution in the rock sample. This technique has a short experimental duration (hours versus days for the through-diffusion approach) and works for the strongly-sorbing tracers that would not break through in the through-diffusion approach.

2.2 LA/ICP-MS analyses

Laser ablation is the process by which an intense burst of energy delivered by short laser pulses is used to vaporize a minute (nanogram-range) sample from a specific location. The

chemical composition of the vaporized sample is then analyzed by an inductively coupled plasma-mass spectrometer. Since 1985, laser ablation coupled with ICP-MS has evolved as a powerful analytical tool for *solid* sampling and analysis (e.g., Russo et al., 2000, 2002; Sylvester, 2005). LA/ICP-MS can simultaneously detect a large number of chemical elements at low detection limits, typically in the range of nanograms to low micrograms per gram.

We used the CETAC LSX-200 laser ablation system (CETAC Technologies, Omaha, NE), interfaced with the X-Series ICP-MS (Thermo Electron Corporation, West Palm Beach, FL). During data acquisition, signal intensities (counts per second, cps) were recorded for a number of elements, including introduced radionuclides (^{234}U, ^{235}U, and ^{237}Np) and other elements intrinsic to the rock (e.g., ^{29}Si, ^{85}Rb, ^{137}Ba, ^{232}Th). After laser firing, there was about a 10-second pause before the ablated sample material was transported to the ICP-MS detector for elemental detection. The signal intensity measured during this period was used to determine the instrument background for each element. When the sample reached the detector, there was a sharp rise in signal intensity, followed by a gradual decrease in intensity to near-background levels within several minutes after laser firing. The integrated signal intensity data were then obtained by adding the signal (after subtracting the background); an Excel macro was constructed for the data reduction. Differences in the integrated signal intensity for different elements reflect their differences in concentration in the sample matrix (Hu et al., 2004). The concentration of an analyte can be quantified by measuring a reference element with a known concentration in both the unknown and reference samples (e.g., NIST Standard Reference Materials). But the disadvantage of the LA/ICP-MS technique is that absolute concentration data are difficult to acquire because the matrix-matched standards are not available. However, as a semi-quantitative survey tool, the technique provides useful insights into compositional

heterogeneities that would be otherwise overlooked during conventional bulk analytical measurements. In this work, we focus on the distribution in the field samples of applied radionuclides at locations relative to the fracture pathways, and we present the results for the uranium ratio and signal response for ^{237}Np. For the laboratory diffusion test, we employed a novel approach of simultaneously analyzing solid samples and a liquid solution containing known elements and concentrations. One of the major element constituents of the sample and reference matrix was chosen (such as ^{29}Si for granite) as the reference element. The normalized ratio of analyte to internal standard for the LA/ICP-MS analysis of both the sample and reference standards (NIST SRM 616, 614, 612, and 610) was then used to calculate the analyte concentration.

3. Results and discussion

3.1. *Detection of actinides in field samples*

A granite slab (ID A6-5) of 300 mm diameter and 35 mm thickness, with several visible advective flow paths impregnated with yellow-colored epoxy resin, is used in this study to map radionuclide distribution; a quarter of the slab containing the major fracture is shown in a photo in Figure 1A. Using γ-spectrometry, this slab sample was measured to a bulk radioactivity of 7.5×10^3 Bq for ^{137}Cs and $<1.28\times10^2$ Bq for ^{60}Co (Möri et al., 2006). Square-shaped sub-samples (32 mm each side, suitable for being placed inside the laser ablation chamber for analyses) were cut (Figure 1B) such that they focus on the regions around the advective flow path so that we could study the spatial distribution of radionuclides there. For this shear zone, the flow path is bounded on one side with a mylonite region of a thickness varying from 7-11 mm, with a thin (0.4 mm thick), black-colored (probably biotite) wall near the fracture (Figure 1D). Mylonite forms by dynamic recrystallization of rock as a response to shear stress and deformation. As the minerals in the coarse-grained granite recrystallize, they generally become smaller in grain size.

The mica-rich mylonite in the GTS granite has a low porosity—about 0.1%—and this wall appears to be even tighter in response to the laser shots. On the other side of the flow path, the granitic matrix has a porosity of about 1%.

Table 1 lists the amount of radionuclides injected in the tracer test in the shear zone two months before the excavation. Most of these radionuclides are relatively short-lived, with high specific activity suitable for radiometric analyses (Gonzales et al., 2005). At the opposite extreme, the actinides applied have extremely long lives and a small mass recovery during the dipole test for the actinides residing in the rock samples. Mass spectrometric analysis will be suitable for detecting their presence in the excavated rock samples.

We performed LA/ICP-MS analyses on the samples to monitor the signal response of various elements, including those intrinsic to the rock (e.g., ^{29}Si, ^{44}Ca, ^{85}Rb, ^{137}Ba, and ^{232}Th) and applied tracers (^{60}Co, ^{90}Sr, ^{137}Cs, ^{234}U, ^{235}U, and ^{237}Np). The low concentrations of fission products (^{60}Co and ^{137}Cs) were effectively masked by isotopic and polyatomic mass interferences. For example, ^{60}Ni has a natural abundance of 26.2% and ^{137}Ba of 11.3%. These isotopes interfere with the measurement of ^{60}Co and ^{137}Cs, respectively. Barium and nickel are expected to have concentrations in a granite as high as several hundred milligrams per kilogram; for example, the reported barium concentration in the granite of Stripa mine of Sweden is 545±60 mg/kg (Nordstrom et al., 1989). This is at least two orders of magnitude higher than the expected concentrations of ^{60}Co and ^{137}Cs, even we assume all the measured radioactivity of these radionuclides in the whole slab is concentrated in a thin layer (1 mm thick) at a fracture (with a 1 mm aperture) with a length of 100 mm. Similarly, we monitored the atomic masses 113 and 152 for injected radionuclides ^{113}Sn and ^{152}Eu, but the isobaric interference of ^{113}Cd and

^{152}Sm, and other polyatomic mass interference, prevents the mass spectrometric detection of these radionuclides at low concentration.

Although similar masking issues may be encountered with actinide species, there are many fewer mass interferences at high mass numbers because of the smaller number of naturally-occurring isotopes in this mass range. Because of the high amount of actinides injected into the shear zone (Table 1), their presence in the fracture interfaces is unambiguously detected, as shown in Figure 1. Long-lived ^{234}U, ^{235}U, and ^{237}Np were detected on flow channels, as well as in the adjacent rock matrix, using the sensitive, feature-based mapping of the LA/ICP-MS technique. Increased activity above natural background was observed both in the water-conducting fracture and in the adjacent rock matrix, which demonstrates the contribution of matrix diffusion to retarding radionuclide transport by removing it from the advective flow path.

3.2. *Structural and mineralogical controls on radionuclide transport*

^{237}Np signal response and ^{235}U/^{238}U ratios were determined on both sides of a fracture that was composed of two different kinds of wall rock: relatively low-porosity mylonite and granite. The highest activities were found within the flow path, and these actinides were detected in the rock matrix (Figure 1C, right side) to a depth of about 7 mm. Some ^{237}Np was observed to pass through the mylonite region to the granitic matrix (Figure 1C, left) to a depth of about 20 mm (Figure 1). The distribution of actinides in the neighboring matrix regions is relatively irregular, indicating grain boundary diffusion in coarsely-grained granite with mineral sizes of several millimeters, which are larger than the sampling spot size for the LA/ICP-MS (0.3 mm). Similar observations were made with the β/γ-autoradiographs, giving clear evidence of grain-boundary-controlled radionuclide retardation sites in the rock matrix (Möri et al., 2006).

Generally, the distribution of ^{235}U and ^{234}U follows that of ^{237}Np, which is consistently detected the furthest from the fracture into the matrix (Figure 1; Tables 2-3). This is related to the

larger apparent diffusivity of neptunium than uranium in the granite, as confirmed by the laboratory diffusion test (discussed later). Due to the very low instrumental background, which was measured to be about 0.5 normalized cps per laser shot (Table 2), and the lack of naturally-occurring ^{237}Np in the sample, LA/ICP-MS can detect even very tiny amounts (about 10^{-4} mg/kg) of injected ^{237}Np remaining in the granite. However, because of the relatively small injected mass, ^{234}U has the smaller (by a factor of 2) detection factor for the ^{234}U/^{235}U ratio, with a ratio of 0.013 in the injected solution and a natural ratio of 0.00764 (Table 2). Similarly, the detection factor for ^{238}U/^{235}U is about 200 for a sampling spot (No. 3 in sub-sample A4) with a ratio of 0.658, indicating a high presence of ^{235}U in this sample location (Table 3).

The fracture wall appears to reduce radionuclide transport into the mylonite region; this is especially clear from the data for ^{237}Np, which has a higher sensitivity and apparent diffusivity than uranium isotopes. While the sampling spot (Table 2, No. 2) at the interface of the fracture and wall in sub-sample A2 is as high as 306 cps, the ^{237}Np signal 500 μm away is only 27.4 cps. The sampling spot (Table 3, No. 2) directly on the fracture wall has a ^{237}Np signal of 71.8 cps, with two sampling spots (Table 3, Nos. 3-4) on the fracture ranging from 261 to 474 cps, and a sampling spot (Table 3, No. 5) on the granitic matrix on the other side of the shear zone has 119 cps. We have recently analyzed more sub-samples, as well as conducted feature-based sampling (i.e., following the walls and regions immediately on both sides of the wall), to further our understanding of the structural and mineralogical controls on radionuclide transport, and data synthesis is underway.

3.3. Laboratory diffusion measurements

Laboratory tests on the diffusion of several tracers into a saturated granite rock were conducted to independently obtain the apparent diffusivity of relevant tracers (Co, Sr, U, and Np) used in the field dipole test. Figure 2 presents the diffusion profiles for these tracers, with

rhenium behaving as the non-sorbing ReO_4^- and nickel as the analog for cobalt. The background line for each tracer is also presented in the figure, with the background signals coming from the tracer's intrinsic presence in the granite, isotopic, and polyatomic mass interferences, or the instrument. Compared with the background levels, the input signal measured at the bottom of the granite sample varies from about two orders of magnitude larger for cesium (with its relatively high concentration in granite—about 1 mg/kg when measured from a clean sample) to more than four orders for neptunium, which has very low interference. Diffusion of non-retarded ReO_4^- has crossed the 10-mm sample length within the diffusion duration of nearly 20 hours. All other tracers have diffusion profiles showing retardation from their interactions with the granite minerals.

We used a numerical simulator, HYDRUS-1D, to fit the diffusion profiles of these tracers. The software package can simulate water, heat, and solute movement in one-dimensional, variably saturated media. The HYDRUS program numerically solves the Richards' equation for variably saturated water flow and convection–dispersion-type equations for solute transport of up to ten independent solutes (Simunek et al., 2005). For our saturated diffusion data, only the apparent diffusivity D_a was fitted, with D_a related to the effective diffusion coefficient D_e of a sorbing solute as follows:

$$D_a = D_e/R. \quad (1)$$

R is the dimensionless retardation factor that accounts for the interaction of the solute with the porous medium. For a linear sorption isotherm and fast sorption (compared to diffusion), $R = 1+(K_d \times \rho_b)/\theta$ and K_d is the equilibrium distribution coefficient. The effective diffusion coefficient $D_e = \delta \times D_0 / \tau$, with τ (the tortuosity, >1) and δ (constrictivity factor, ≤1; only

important in narrow pores) related to the geometry of the porous media and D_0 the aqueous molecular diffusion coefficient of the diffusant (Hu and Wang, 2003).

Fitted apparent diffusivity, a term that includes effective diffusivity, retardation factor, and tortuosity, is 8.3×10^{-11} m^2/s for ReO_4^-, 1.7×10^{-13} m^2/s for nickel and ^{235}U, and 8.3×10^{-13} m^2/s for cesium and ^{237}Np. Fitted diffusion profiles are compared with the experimental data in Figure 3. The fitting captured the data fairly well for tracers other than ReO_4^-; note the semi-log plot of Figure 3. In coarse-grained granite with micro-fractures, diffusion probably occurs in more than one pathway; a dual-rate diffusion model would have described the data better. However, the apparent diffusivity measured in this preliminary study is comparable to those obtained with a through-diffusion method in the GTS granite sample, with a diffusion coefficient of 8.3×10^{-11} m^2/s for tritium and 4.3×10^{-14} m^2/s for cesium (Havlova, 2007, Nuclear Research Institute, Czech Republic, personal communication). Using a tortuosity value of 112, calculated from the measured D_a and reported D_0 of tritium, we can obtain the K_d values of sorbing tracers, assuming that linear and fast sorption are applicable. This, however, is not the focus of this study.

3.4. Prediction of in situ *diffusion in field dipole test*

Based on measured D_a, we can compare the predicted diffusion distances with those measured using the samples collected from the field dipole test. For a semi-infinite system in which the concentration profile does not reach the end of the sample, the analytical solution to the transient diffusion equation (Fick's second law) is as follows (Crank, 1975; Flury and Gimmi, 2002):

$$\frac{C}{C_0} = \frac{1}{2} erfc \frac{x}{2\sqrt{D_a \times t}} \qquad (2)$$

where C (M L^{-3}) is the observed concentration at location x based on an initial concentration C_0 (M L^{-3}), C/C_o is the relative concentration, x (L) is the diffusion distance, and t (T) is the diffusion time. Using collimated γ-spectrometry with the spatial resolution of several millimeters, Möri et al. (2006) reported maximum ^{137}Cs diffusion into the rock matrix adjacent to a water-conducting fracture to a depth of 45 mm within 3 years and for ^{60}Co to about 3 mm in 2 months. In this study, we obtain a conservative diffusion distance of about 4.5 mm for both uranium and neptunium in the granite region near the fracture within 2 months (Figure 1).

Table 4 presents the comparison of the measured diffusion distance in the field dipole test for four tracers with the predicted distance using the analytical solution of Equation 2 and laboratory-derived diffusion coefficients. Given the limited data, it is encouraging that comparison shows the numbers to be fairly similar. More data collection and analysis of the spatial distribution of radionuclides in the fracture interface zones that encompass a variety of structural and mineralogical features is currently underway.

4. Summary and conclusions

We analyzed fractured granite samples from a dipole tracer test at the GTS to study the diffusion profiles of injected radionuclides across the fracture interface zones. Long-lived ^{234}U, ^{235}U, and ^{237}Np were detected in flow channels, as well as in the adjacent rock matrix, using the sensitive, feature-based mapping of the LA/ICP-MS technique. The major water-conducting fracture studied in this work is bounded by mylonite on one side and granitic matrix on the other. Because of the low porosity, hydraulic conductivity, and diffusivity of the fracture wall and the mylonite region itself, these actinides did not penetrate into the mylonite side as much as the relatively higher-porosity granite matrix. Overall, the maximum penetration depth detected with

this technique for ^{237}Np in the granite matrix was up to 10 mm over the 60-day field experiment time scale, illustrating the importance of matrix diffusion in retarding radionuclide transport from the advectively-flowing fractures. Laboratory tests and numerical modeling of radionuclide diffusion into granitic matrix was conducted to complement and help interpret the field results. Measured apparent diffusivity of multiple tracers in granite provides consistent predictions for radionuclide transport in the fractured granitic rock. Further analyses of the rock samples are in progress and insights obtained will help the planning and execution of long-term diffusion tests currently underway at the GTS.

Acknowledgments

This work was primarily supported by the following partners of the Long Term Diffusion (LTD) project for Phase VI of the GTS: Japan Atomic Energy Agency (JAEA) and National Institute of Advanced Industrial Science and Technology (AIST) of Japan, Radiation and Nuclear Safety Authority (STUK) and University of Helsinki in Finland, Nuclear Research Institute of Czech Republic, and NAGRA of Switzerland. Financial support from the United States Department of Energy (DOE), Office of Civilian Radioactive Waste Management (OCRWM), and the Office of Chief Scientist (OCS) is also acknowledged. The views, opinions, findings, and conclusions or recommendations expressed herein do not necessarily state or reflect those of the DOE/OCRWM/OCS. This work was performed under the auspices of the U.S. Department of Energy by the University of California, Lawrence Livermore National Laboratory, under Contract W-7405-Eng-48.

References

1 Abelin, H., Birgersson, L., Moreno, L., Widen, H., Agren, T., Neretnieks, I., 1991. A large-scale
2 flow and tracer experiment in granite. 2. Results and interpretation. Water Resour. Res. 27,
3 3119–3135.

4 Alexander, W.R., Bradbury, M.H., McKinley, I.G., Heer, W., Eikenberg, J., Frick, U., 1992. The
5 current status of the radionuclide migration experiment at the Grimsel underground rock
6 laboratory. Sci. Basis Nucl. Waste Manage. XV, 721–728.

7 Brookins, D.G., 1986. Rhenium as analog for fissiogenic technetium: Eh-pH diagram (25 oC, 1
8 bar) constraints. Appl. Geochem. 1, 513–517.

9 Crank, J., 1975. The Mathematics of Diffusion. 2nd ed., Oxford University Press Inc., New
10 York.

11 Dai, Z., Wolfsberg, A., Lu, Z., Reimus, P., 2007. Upscaling matrix diffusion coefficients for
12 heterogeneous fractured rocks. Geophy. Res. Lett. Vol. 34, L07408,
13 doi:10.1029/2007GL029332.

14 Eikenberg, J., Ruethi, M., Alexander, W.R., Frieg, B., Fierz T., 1998. The excavation project in
15 the Grimsel Test Site—In situ high resolution gamma and alpha spectrometry of Co-60, Se-
16 75, Sn-113, Eu-152 and Np-237/Pa-233. MRS Symp. Proc. 506, 655–662.

17 Flury, M., Gimmi, T.F., 2002. Solute Diffusion. In Methods of Soil Analysis. Part 4—Physical
18 Methods. J.H. Dane and G.C. Topp (eds.). Soil Sci. Soc. Am., Madison, WI, pp. 1323–1351.

19 Frieg B., Alexander W.R., Dollinger H., Bühler C., Haag P., Möri A., Ota K., 1998. In situ
20 impregnation for investigating radionuclide retardation in fractured repository host rocks. J.
21 Contam. Hydrol. 35, 115–130

22 Gonzales, E.R., Garcia, S.R., Mahan, C., Hang, W., 2005. Evaluation of mass spectrometry and
23 radiation detection for the analysis of radionuclides. J. Radioanal. Nucl. Chem. 263, 457–
24 465.

25 Grathwohl, P., 1998. Diffusion in Natural Porous Media: Contaminant Transport,
26 Sorption/Desorption and Dissolution Kinetics. Kluwer Academic Publishers, Boston, MA.

27 Grisak G.E., Pickens J.F., 1980. Solute transport through fractured media. Part I: the effect of
28 matrix diffusion. Water Resour. Res. 16, 719–730

29 Hadermann, J., Heer, W., 1996. The Grimsel (Switzerland) migration experiment: Integrating
30 field experiments, laboratory investigations and modelling. J. Contam. Hydro. 21, 87–100.

31 Hu, Q. H. and Wang, J.S.Y., 2003. Aqueous-phase diffusion in unsaturated geologic media: A
32 review. Crit. Rev. Environ. Sci. Technol. 33, 275–297.

33 Hu, Q., Salve, R., Stringfellow, W.T., Wang, J.S.Y., 2001. Field tracer transport tests in
34 unsaturated fractured tuffs. J. Contam. Hydro. 51, 1–12.

Hu, Q., Kneafsey, T.J., Wang, J.S.Y., Tomutsa, L., Roberts, J.J., 2004. Characterizing unsaturated diffusion in porous tuff gravels. Vadose Zone J. 3, 1425–1438.

Lide, D.R., Ed., 2000. CRC Handbook of Chemistry and Physics. Boca Raton, Florida, CRC Press.

Maloszewski, P., Zuber, A., 1993. Tracer experiments in fractured rocks—Matrix diffusion and the validity of models. Water Resour. Res. 29(8), 2723–2735.

Meigs, L.C., Beauheim, R.L., 2001. Tracer tests in a fractured dolomite. 1. Experimental design and observed tracer recoveries. Water Resour. Res. 37, 1113–1128.

Möri, A., Biggin, C., Mäder, U., Eikenberg, J., Rüthi M., 2006. Phys. Chem. Earth 31(10–14), 511–516. Mori, A., Biggin, C., Mader, U., Eikenberg, J. and Ruthi, M. 2006. Novel application of β/γ autoradiography and collimated γ-spectrometry to study in situ radionuclide migration paths in fractured rock. Phys. Chem. Earth, Parts A/B/C 31, 511–516.

Neretnieks I., 1980. Diffusion in the rock matrix: an important factor in radionuclide migration? J. Geophys. Res. 85, 4379–4397

National Research Council (NRC), 2000. Research Needs in Subsurface Science. U.S. Department of Energy's Environmental Management Science Program. The National Academies Press, Washington, D.C.

Nordstrom, D.K., Olsson, T., Carlsson, L. and Fritz, P. 1989. Introduction to the hydrogeochemical investigations within the International Stripa Project. Geochimica et Cosmochimica Acta 53(8): 1717–1726.

Novakowski, K.S., Lapcevic, P.A., 1994. Field Measurement of Radial Solute Transport in Fractured Rock. Water Resour. Res, 30, 37–44.

Ota K., Moeri A., Alexander W., Frieg B., Schild M., 2003. Influence of the mode of matrix porosity determination on matrix diffusion calculations. J. Contam. Hydrol. 61, 131–145.

Russo, R.E., Mao, X.L. Borisov, O.V., Liu, H.C., 2000. Laser ablation in atomic spectroscopy. Encyclopedia of Analytical Chemistry: Instrumentation and Applications. Chichster, John Wiley & Sons Ltd.

Russo, R.E., Mao, X.L., Liu, H.C., Gonzalez, J., Mao, S.S., 2002. Laser ablation in analytical chemistry—A review. Talanta, 57, 425–451.

Sardini, P., Siitari-Kauppi, M., Beaufort, D., Hellmuth, K.H., 2006. On the connected porosity of mineral aggregates in crystalline rocks. Am. Mineral. 91, 1069–1080.

Salve, R., Liu, H.H., Cook, P., A.Czarnomski, Hu, Q., Hudson, D., 2004. Unsaturated flow and transport through a fault embedded in fractured welded tuff. Water Resour. Res. Vol. 40, W04210, doi: 10.1029/2003WR002571.

Simunek, J., van Genuchten, M.Th. and Sejna, M., 2005. The HYDRUS-1D Software Package for Simulating the Movement of Water, Heat, and Multiple Solutes in Variably Saturated Media, Version 3.0, HYDRUS Software Series 1, Department of Environmental Sciences, University of California Riverside, Riverside, CA, USA, 270 pp.

Smith, P.A., Alexander, W.R., Kickmaier, W., Ota, K., Frieg, B., McKinley, I.G., 2001. Development and testing of radionuclide transport models for fractured rock: examples from the Nagra/JNC Radionuclide Migration Programme in the Grimsel Test Site, Switzerland. J. Contam. Hydro. 47, 335–348.

Sylvester, P.J., 2005. Laser ablation ICP-MS developments and trends for 2003. Geostandard Geoanal. Res. 29, 41–52.

Zhang, P.C., Brady, P.V., 2002. Introduction to properties, sources and characteristics of soil radionuclides. Zhang P.C. and P.V. Brady (ed.), Geochemistry of soil radionuclides. SSSA Special Publication Number 59, Madison, WI, pp.1–20.

Zhou, Q.L., Liu, H.H., Bodvarsson, G.S., Molz, F.J., 2006. Evidence of multi-process matrix diffusion in a single fracture from a field tracer test. Transp. Porous Media 63, 473–487.

Table 1 Compilation of relevant radionuclides used in dipole test at the GTS [a]

Radionuclide	Half-life (yr) [b]	Injected amount		Mass recovery
		Radioactivity (Bq)	Mass (nmol)	
^{60}Co	5.27	$(2.03\pm0.05)\times10^{6}$	0.808	10%
^{75}Se	0.328	$(1.08\pm0.08)\times10^{7}$	0.267	90%
^{113}Sn	0.315	$(1.93\pm0.10)\times10^{6}$	0.0459	A few percent
^{137}Cs [c]	30.2	1.88×10^{7}	42.7	70-100%
^{152}Eu	13.5	$(2.96\pm0.10)\times10^{5}$	0.302	A few percent
^{233}Pa [d]	0.0739	$(5.80\pm0.40)\times10^{5}$	0.00324	~5%
^{234}U	246,000	$(5.74\pm0.37)\times10^{5}$	10,677	~5%
^{235}U	704,000,000	$(1.54\pm0.10)\times10^{4}$	819,810	~5%
^{237}Np	2,144,000	$(5.80\pm0.60)\times10^{5}$	94,033	~5%

[a] Injected radioactivity in becquerel (Bq) and mass recovery rates during the pulsed injection of radionculdies in the dipole test are from Eikenberg et al. (1998).

[b] From Lide (2000).

[c] Three tracer tests were carried out in 1993, injecting ^{137}Cs each time between 6.0×10^{6} and 6.0×10^{6} Bq and recovery of 70–100% at the extraction borehole within the first 1,000 hours (Möri et al., 2006).

[d] Short-lived progeny ^{233}Pa in secular equilibrium with its long-lived parent ^{237}Np in the injected solution.

Table 2 Radionuclide detection at six sampling spots across the fracture interface zone in a granite sub-sample A2 [a]

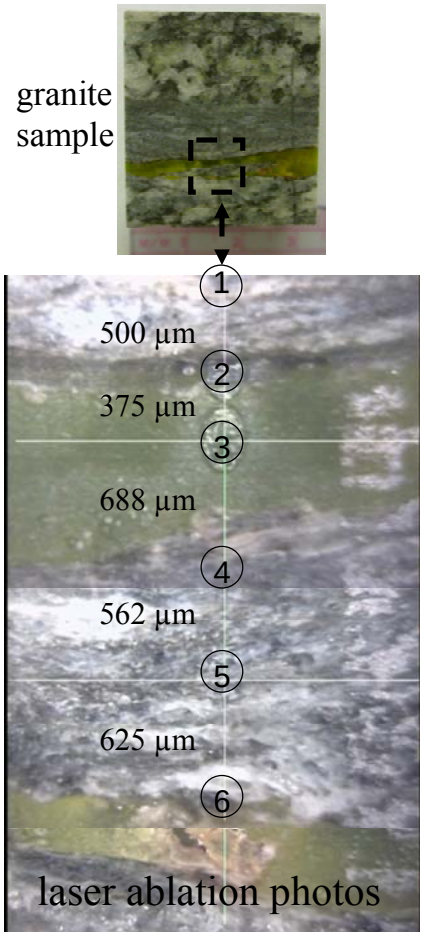

Sampling spot	$^{238}U/^{235}U$	$^{234}U/^{235}U$	^{237}Np (cps)
1 (mylonite)	109	0.0116	27.4
2 (wall / fracture)	61.1	0.0096	306
3 (fracture)	13.1	0.0157	29.4
4 (matrix)	132	0.0082	51.3
5 (matrix)	49.4	0.0131	85.9
6 (matrix / fracture)	8.23	0.0116	402
Natural	138	0.00764	~0.5
Tracer	< 1(?)	0.0130	3462

[a] This sub-sample A2 (32 mm each side) has two water-conducting fractures (apertures about 1 and 0.4 mm). Photos taken during the laser ablation for each sampling spot, along with the distance between the spots, are shown to the left. The type of spots sampled is indicated (matrix: granite; wall: fracture wall; fracture: advective flow path impregnated by the resin which may contain fracture infill and corresponding radionuclide ratios presented in the tabulated format. Included also has the expected ratios in nature and from injected radioactivity.

Table 3 Radionuclide detection at eight sampling spots across the fracture interface zone in a granite sub-sample A4 [a]

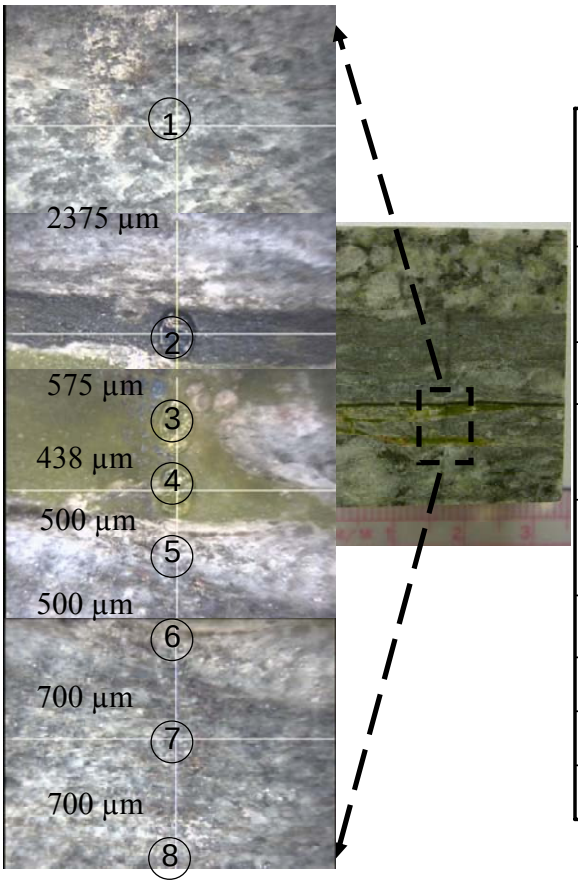

Sampling spot	$^{238}U/^{235}U$	$^{234}U/^{235}U$	^{237}Np (cps)
1 (mylonite)	152	0.0221	38.6
2 (wall)	24.0	0.0077	71.8
3 (fracture)	0.658	0.0146	474
4 (fracture)	4.28	0.0127	261
5 (matrix)	94.0	0.0143	119
6 (matrix)	113	0.0060	46
7 (matrix)	130	0.0093	28.8
8 (matrix)	52.0	0.0106	15.8

[a] The granite sub-sample A4 (32 mm each side) has a water-conducting fracture of ~1 mm wide.

1 Table 4 Comparison of measured and predicted diffusion distance

Element	Apparent diffusivity (m^2/s)	Diffusion time (month)	Relative concentration	Diffusion distance (mm)	
				Measured	Predicted
Co; Ni	1.7×10^{-13}	3	0.005	3	3.7
Cs	8.3×10^{-13}	36	0.001	43	41
U	1.7×10^{-13}	3	0.05	4.5	2.6
Np	8.3×10^{-13}	3	0.05	4.5	6.0

Figure Captions

Figure 1 Sample processing steps (A→B→C) and measured transverse profile for $^{235}U/^{238}U$ ratio and ^{237}Np signal (normalized cps per laser pulse) across the fracture interface zone; indicated on the figure are the corresponding mineralogical regions. Dashed line is the natural $^{235}U/^{238}U$ ratio of 0.0072. The circled data in the granite region is used to compare with the predicted diffusion distance.

Figure 2 Experimental data of tracer diffusion profile in saturated granite. Solid lines are the averaged source concentrations measured at the bottom (diffusion interface is zero) for tracers, and dashed lines are the averaged background levels of tracers.

Figure 3 Experimental data and fitted curves of tracer diffusion in the saturated granite.

Figure 1

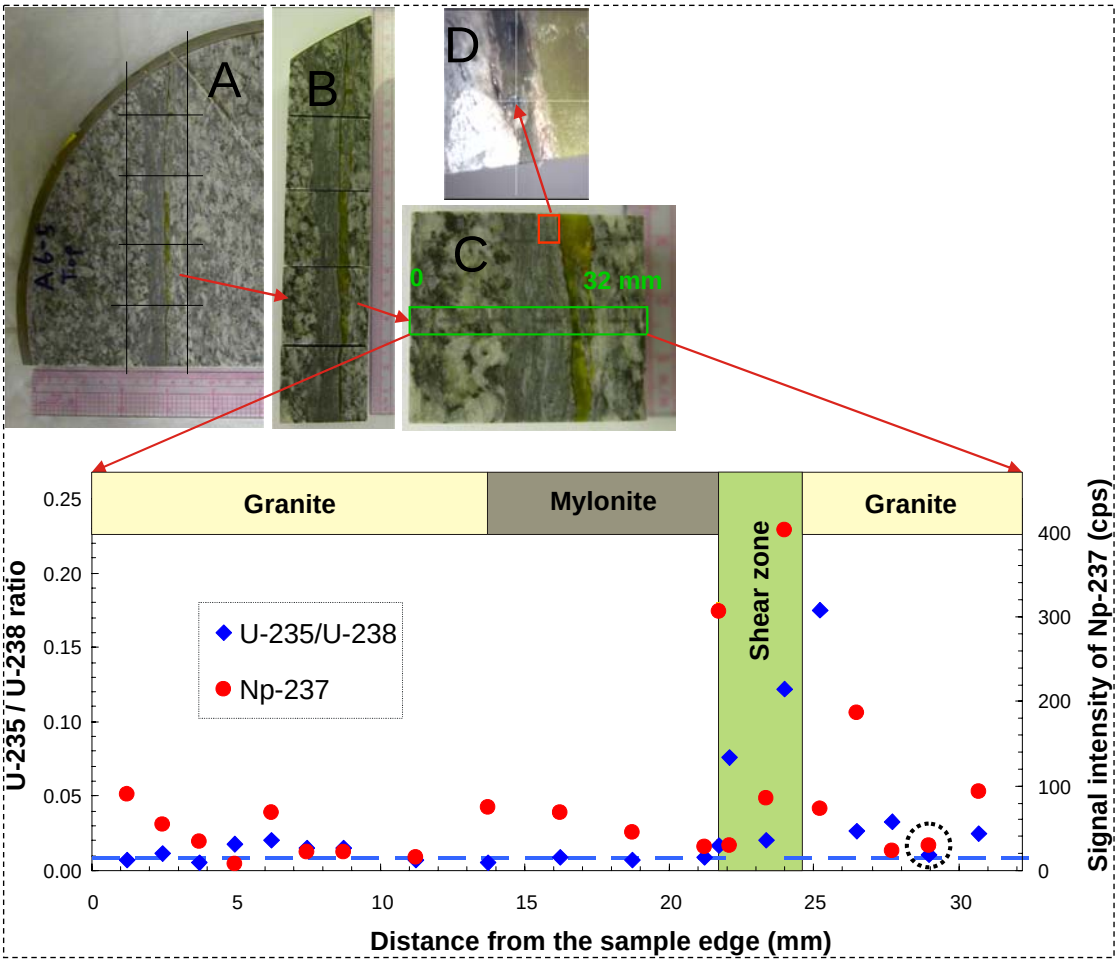
A
B
C
D
0
32 mm
Granite
Mylonite
Granite
Shear zone
U-235/U-238
Np-237
U-235 / U-238 ratio
Signal intensity of Np-237 (cps)
Distance from the sample edge (mm)
0.25
0.20
0.15
0.10
0.05
0.00
400
300
200
100
0
0
5
10
15
20
25
30

Figure 2

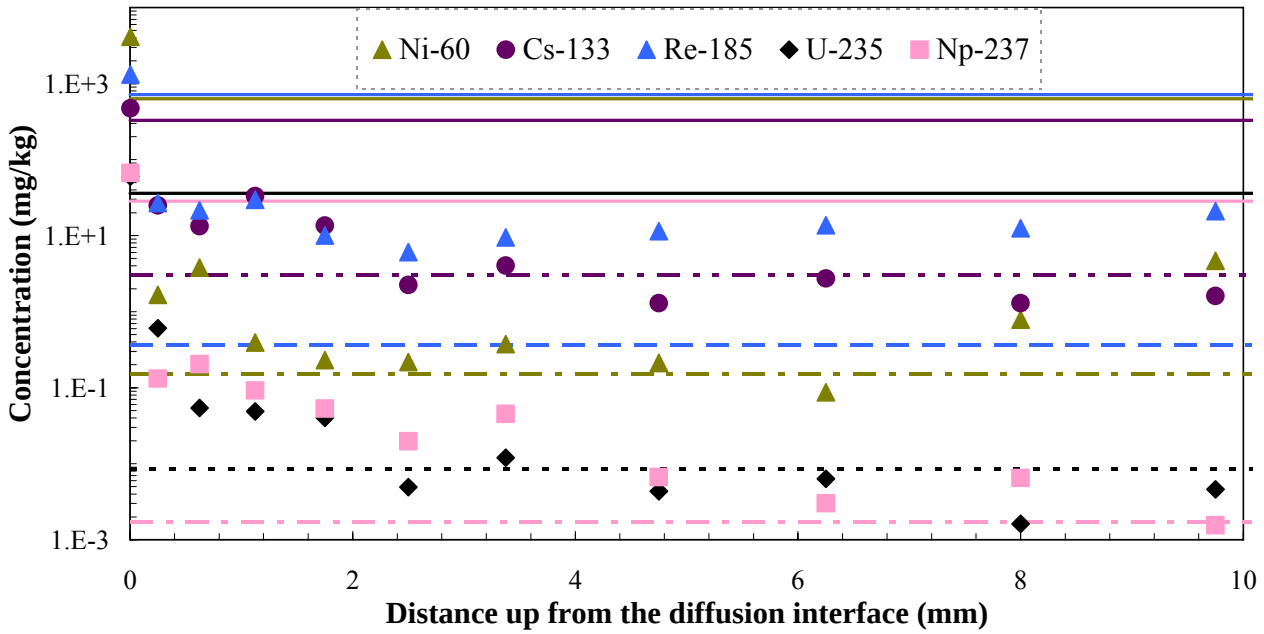
Ni-60
Cs-133
Re-185
U-235
Np-237
1.E+3
1.E+1
1.E-1
1.E-3
Concentration (mg/kg)
0
2
4
6
8
10
Distance up from the diffusion interface (mm)

Figure 3

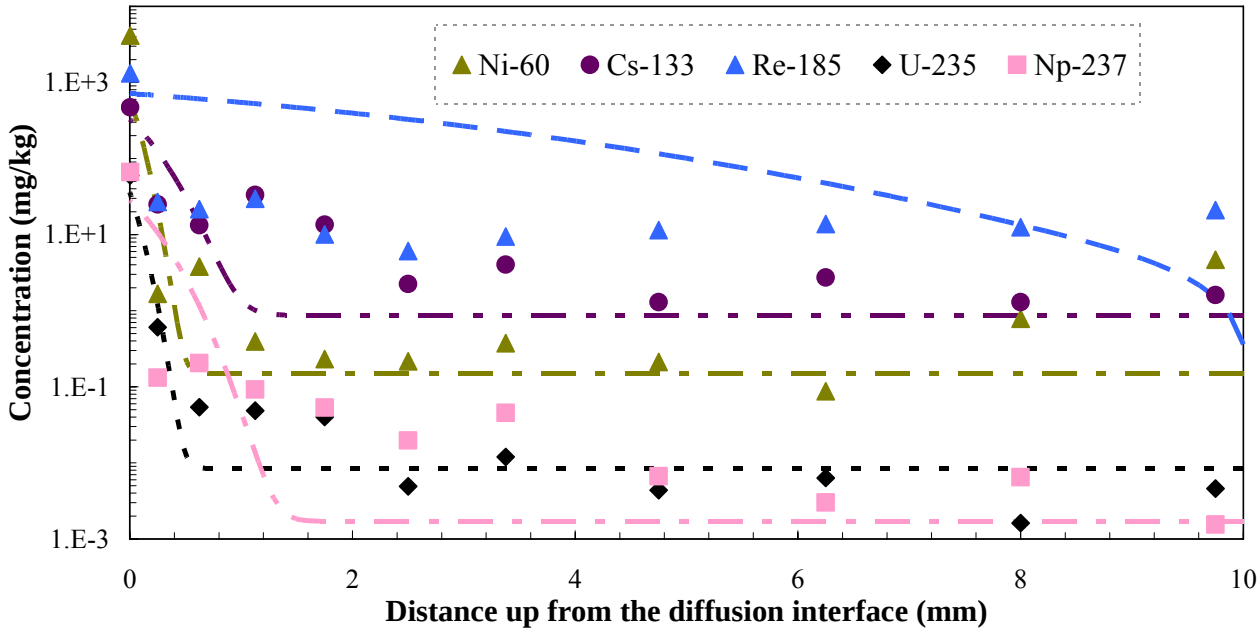
Ni-60
Cs-133
Re-185
U-235
Np-237
1.E+3
1.E+1
1.E-1
1.E-3
Concentration (mg/kg)
0
2
4
6
8
10
Distance up from the diffusion interface (mm)